Plasma-sprayed Al_2O_3-TiB_2-SiC ternary composite coatings and its wear behaviour based on SiC content

Mirhosseini, Seyed Hossein; Mosallaee, Masoud; Razavi, Mansour; Fotouhi, Mohammad

DOI
10.1080/17515831.2023.2232990

Publication date
2023

Document Version
Final published version

Published in
Tribology - Materials, Surfaces and Interfaces

Tribology - Materials, Surfaces & Interfaces

ISSN: (Print) (Online) Journal homepage: https://www.tandfonline.com/loi/ytrb20

Plasma-sprayed Al_2O_3-TiB_2-SiC ternary composite coatings and its wear behaviour based on SiC content

Seyed Hossein Mirhosseini, Masoud Mosallaee, Mansour Razavi & Mohammad Fotouhi

To cite this article: Seyed Hossein Mirhosseini, Masoud Mosallaee, Mansour Razavi & Mohammad Fotouhi (2023): Plasma-sprayed Al_2O_3-TiB_2-SiC ternary composite coatings and its wear behaviour based on SiC content, Tribology - Materials, Surfaces & Interfaces, DOI: 10.1080/17515831.2023.2232990

To link to this article: https://doi.org/10.1080/17515831.2023.2232990

TRIBOLOGY - MATERIALS, SURFACES & INTERFACES
https://doi.org/10.1080/17515831.2023.2232990

I·M3 Institute of Materials, Minerals & Mining
Taylor & Francis Taylor & Francis Group

RESEARCH ARTICLE

Plasma-sprayed Al_2O_3-TiB_2-SiC ternary composite coatings and its wear behaviour based on SiC content

Seyed Hossein Mirhosseini[a], Masoud Mosallaee[a], Mansour Razavi[b] and Mohammad Fotouhi[c]

[a]Department of Mining and Metallurgical Engineering, Yazd University, Yazd, Iran; [b]Department of Ceramic, Materials and Energy Research Center, Karaj, Iran; [c]Department of Materials, Mechanics, Management and Design, Delft University of Technology, Delft, the Netherlands

ABSTRACT

This paper aims to study the effect of adding different SiC content on the wear performance of Al_2O_3-TiB_2-SiC ternary composite coatings produced by the air plasma spraying process. The study used SHS powders as primary materials, consisting of H_3BO_3, Al, and TiO_2, and 5, 10, and 15 Vol.% SiC. The microstructure and wear specifications of the coatings were characterised using FESEM, microhardness, and pin-on-disk methods. The results showed that the addition of SiC led to higher hardness and lower wear track width and rate compared to Al_2O_3-TiB_2 composite coatings. The best wear behaviour was observed in Al_2O_3-TiB_2-10%SiC and 15 wt% SiC composite coatings. The main wear mechanisms were found to be brittle fracture, delamination and adhesive for all samples.

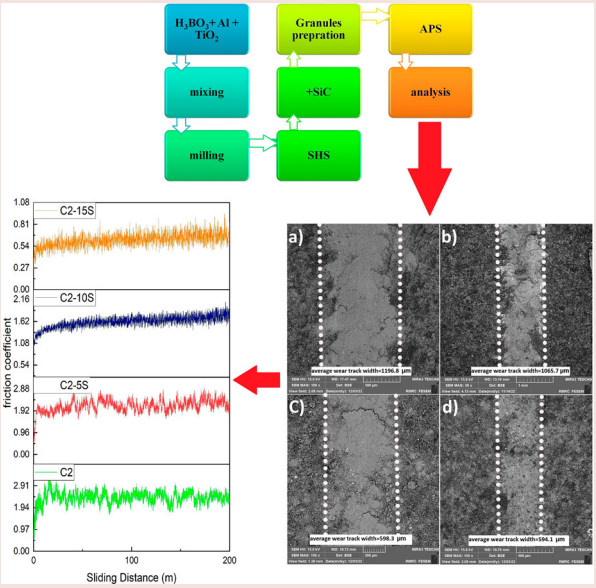

ARTICLE HISTORY
Received 18 March 2023
Accepted 30 June 2023

KEYWORDS
Ceramic coatings; friction; plasma spray; rietveld refinement; wear mechanism; TiB2; Al2O3; SiC; ceramic coatings; Friction; plasma spray; Rietveld refinement; wear mechanism

1. Introduction

Al_2O_3-based composite coatings are utilised in the aerospace, automotive, and petrochemical industries to modify the surface of steel [1]. Alumina coatings possess both high hardness and chemical stability [2]. However, their low thermal shock resistance and fracture toughness are significant drawbacks, making them unsuitable for use in their pure form. It has been established that adding oxide or non-oxide substances to Al_2O_3 can enhance its mechanical properties, making the combination of oxide and non-oxide additives a desirable option [3].

Besides Al_2O_3, other materials known for their hardness, such as TiB_2, TiC, and SiC, have gained attention in the field of surface engineering due to their high hardness and resistance to wear. Furthermore, multi-component ceramic composites have been found to possess higher fracture toughness compared to single component ceramics [4]. Reinforcing agents such as TiC, TiN, ZrO_2, and SiC are employed to improve the structure and mechanics of the Al_2O_3-based composite ceramics [5]. Additionally, these Al_2O_3-TiB_2 coatings have been strengthened with the introducing of TiC and TiN [6–8].

SiC ceramics are known for their resistance to oxidation, corrosion, and creep, as well as their high hardness and wear resistance. Adding SiC to the Al_2O_3 matrix leads to an increase in hardness (Ko

CONTACT Masoud Mosallaee mosal@yazd.ac.ir

Table 1. Specifications of the raw materials.

Materials	Company	Average particle size (μm)
TiO_2	SDfine Art: 40446	<44
H_3BO_3	Merck – 100165	<100
Al	Avl metal – FLPN25	<25
SiC	Industrial	<10
NiCrAlY	Oerlikon metco	−106+53

et al [9].). Zhou et al. reported that SiC addition to Al_2O_3 causes improvements in mechanical properties like hardness, fracture toughness, flexural strength, and surface finish. The wear rate also reduced in comparison with monolithic alumina [10]. Additionally, Al_2O_3-SiC-TiC composites have been shown to have better wear resistance than Al_2O_3 alone (Smirnov et al. [11,12]).

Among these papers, only a few papers discussed the synergetic roles of SiC on the properties of the Al_2O_3-TiB_2-based composites [13,14]. Jianxin [15] fabricated Al_2O_3-TiB_2-SiC_w bulk composites by SiC whiskers, and studied the friction and wear behaviour of them, and found that adding 30 wt% SiC whiskers resulted in a wear rate reduction of less than 10^{-7} mm^3/N.m. They showed that increasing the amount of SiC increased the hardness and the fracture toughness of the samples.

Laser technology has also been utilised in the development of hard and wear-resistant TiB_2-TiC-Al_2O_3-SiC composite coatings on AISI 1020 steel (Masanta et al. [16]). An increase in SiO_2+C content in precursors, was found to increase the micro-hardness of the coating at the cross-section.

The development of Al_2O_3-TiB_2 composite coatings has been achieved through various techniques, including reactive spraying, electron beam deposition, laser cladding, in-situ plasma spray, and axial plasma spray [10,17–24]. Compared to these methods, the atmospheric plasma spraying (APS) method has advantages such as controlled coating thickness, high efficiency, the ability to apply high temperature coatings and cost-efficient and easy use [25]. This simple technology allows for creating coatings with high hardness and excellent wear resistance. For example, Xu et al. [26] deposited Al_2O_3-TiB_2-TiC/Al composite coatings on MB26 magnesium alloy, while Zou et al.

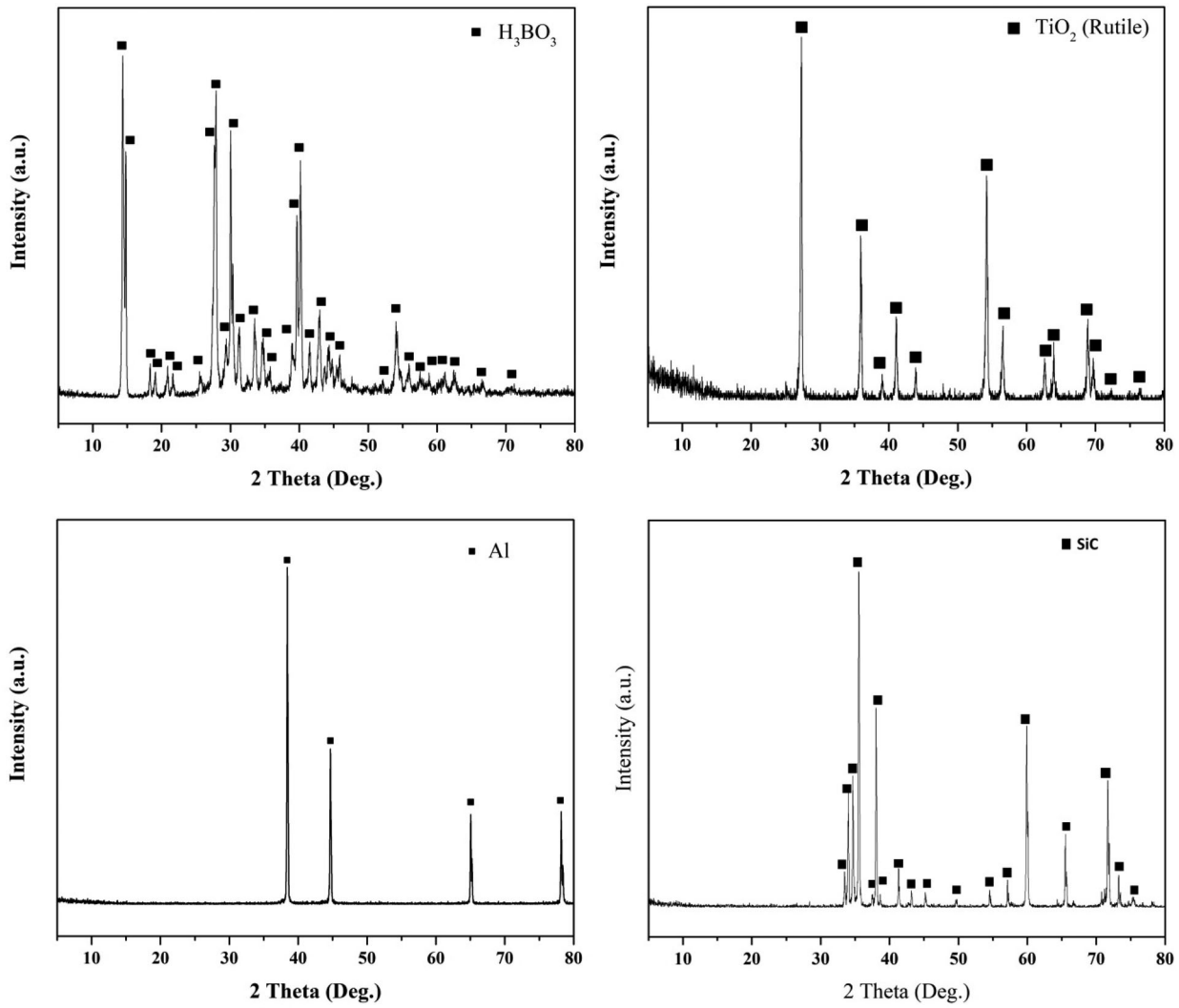

Figure 1. XRD patterns of the starting materials.

Table 2. APS parameters for coatings.

Gun Type	Argon low rate (SCFH)	Hydrogen gas flow rate (SCFH)	Current (A)	Voltage (V)	Powder feed rate (Lbs./Hr.)	Spary distance (Cm)
3MB Metco	80	15	500	55	25	8

[27] developed TiB_2-SiC coatings using a supersonic atmospheric plasma spray process. The spraying conditions affect the coating characteristics, and the process parameters optimised accordingly. Luo et al. [28] produced Al_2O_3-TiB_2/Ni composite-phase surface coatings on Cu-Cr-Zr alloy electrodes using electro-spark deposition.

Another method for producing Al_2O_3-TiB_2 composite powder is self-propagating high-temperature synthesis (SHS). This composition can be synthesised in situ from raw materials, including H_3BO_3, Al, and TiO_2 [29–31].

To the authors' understanding, the impact of SiC content on the wear properties and friction behaviour of APSed Al_2O_3-TiB_2-based composite coatings was not examined before. In this work, the Al_2O_3-TiB_2 composite mixture was synthesised by the SHS method. 5, 10, and 15 vol. % SiC have been added to Al_2O_3-TiB_2 coatings, which were fabricated by the APS. The hardness, friction, and wear properties of the three ternary composite coatings (sliding against WC counterpart) were investigated and compared with the Al_2O_3-TiB_2 coating. Based on the results and observations, the effect of different SiC content on the wear mechanisms of the coatings produced through APS method was discussed. It is expected that this research would shed some light on the design of APSed Al_2O_3-TiB_2 coatings.

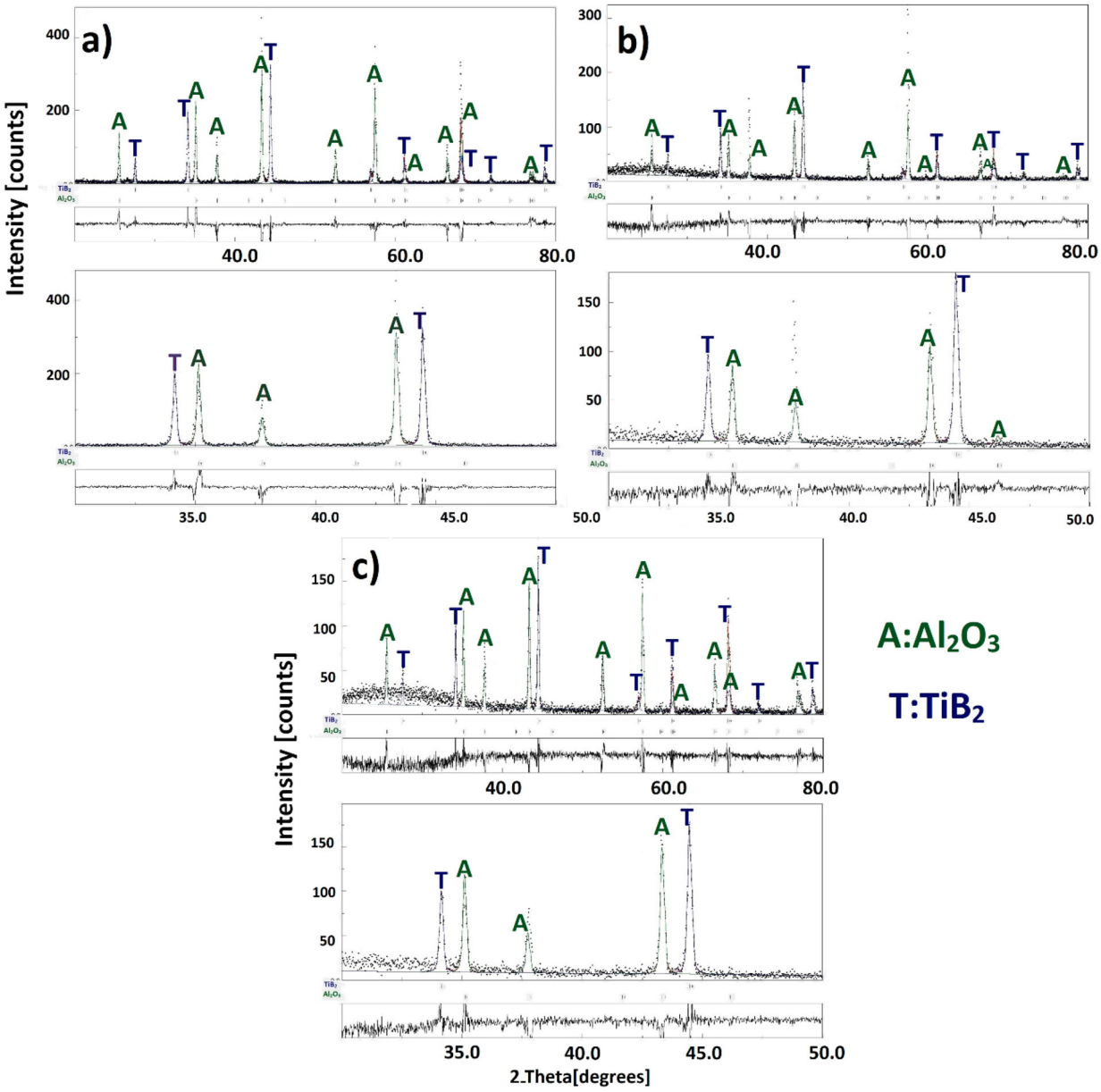

Figure 2. Rietveld refinement results of the synthesised materials milled for (a) 1.5 h, (b) 3 h, (c) 6 h.

Table 3. Quantitative and crystallographic analysis of synthesised powders obtained by Rietveld refinement method.

Milling time	Identified phases	Phase weight fraction (wt%)		Crystal system	Space group	Unit cell dimensions			
		Before SHS	After SHS			a = b (nm)	c (nm)	α = β	γ
1.5 h	Al_2O_3	0	73.61	trigonal	R-3c:H	4.7586503	12.992093	90	120
	TiB_2	0	26.39	hexagonal	P6/mmm	3.028308	3.2302449	90	120
3 h	Al_2O_3	0	71.45	trigonal	R-3c:H	4.756157	12.9853945	90	120
	TiB_2	0	28.55	hexagonal	P6/mmm	3.0273445	3.2275958	90	120
6 h	Al_2O_3	0	73.73	trigonal	R-3c:H	4.761842	12.999987	90	120
	TiB_2	0	26.27	hexagonal	P6/mmm	3.0282197	3.2303743	90	120

2. Materials and methods

2.1. Raw materials and coatings formation process

The specifications for the starting materials are outlined in Table 1. The XRD pattern of the materials used in the research is displayed in Figure 1. The H_3BO_3, Al, and TiO_2 raw powder materials were blended in precise proportions based on reaction 1 [29], and then dry milled using a planetary ball mill at 200 rpm with a 10:1 ball-to-powder ratio in a stainless steel container for 1.5, 3, and 6 h. The resulting mixture was cold-pressed uniaxially into 3 cm diameter stainless steel molds to create raw disks with a theoretical density of approximately 70%. The SHS process was carried out in an electrical furnace under an argon atmosphere at 1000°C.

$$10Al + 3TiO_2 + 6H_3BO_3 \rightarrow 3TiB_2 + 5Al_2O_3 + 9H_2O \quad (1)$$

$$\Delta H_{(298)} = -2518.9\ (KJ/mol)$$

After the combustion synthesis process, the synthesised powder was characterised by XRD (Siemens D-500 X-ray diffractometer equipped with CuKα radiation (λ = 1.54 Å at 20 kV and 30 mA)) and Field emission scanning electron microscopy (TESCAN MIRA3, Czech Republic). Then SiC powder was added to the synthesised powder in amounts of 5, 10, and 15 weight percentages and the specimens were called C2-5S, C2-10S, and C2-15S, respectively. The Al_2O_3-TiB_2 coating was prepared and called C2. Final mixtures were spray dried and granulated, and final granules were air plasma sprayed on a steel disk coated by a NiCrAlY interface layer before final APS to reach out better adherence between the composite coating and metallic substrate. APS processing parameters are summarised in Table 2.

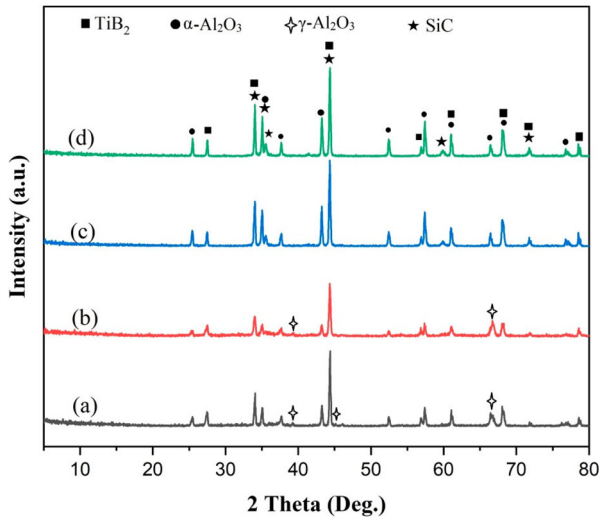

Figure 3. XRD patterns of the coated specimens: (a) C2, (b) C2-5S, (c) C2-10S, (d) C2-15S.

2.2. Coatings specification

The Phase identification of composite coatings was performed by XRD. Vickers indentation technique (MVK-H21, Akashi, Japan) was applied for microhardness measurements with a load of 10 g and a holding time of 15 s. The hardness values were obtained by calculating the mean of at least 5 indentations for each sample. The surface roughnesses of the specimens were specified by TR-100 surface roughness tester. The evaluation of the wear behaviour of composite coatings was conducted by a Pin-on-disk setup [32]. A tungsten carbide (WC) pin (diameter = 5 mm, hardness = 75 HRC) was utilised as the counterbody. The sliding speed during experiments applied normal load and sliding distance were 0.07 m/s, 3 N, and 200 m, respectively. The distance of the WC pin from the centre of the specimens was balanced to be 10 mm (internal diameter: 20 mm). The coefficient of friction during the test was monitored by sensors. The wear rate was calculated by equations 2 and 3 [33]:

$$\text{Wear rate} = V/(N.S) \quad (2)$$

$$V\ (\text{Volume loss}) = (\pi Rd3)/6r \quad (3)$$

Where 'V' is the volume loss of the sample (mm^3), 'N' is the normal load (N), and 'S' is the sliding distance (m). The volume loss was determined from relation 2: Where 'R' is the wear track radius (mm), 'd' is the wear track width (mm), and 'r' is the pin radius (mm) after wear tests.

Rietveld refinement method was applied to study the crystallographic features using Material Analysis Using Diffraction (MAUD) software [34]. The microstructure and worn surfaces of the coatings were analysed by field emission scanning electron microscopy

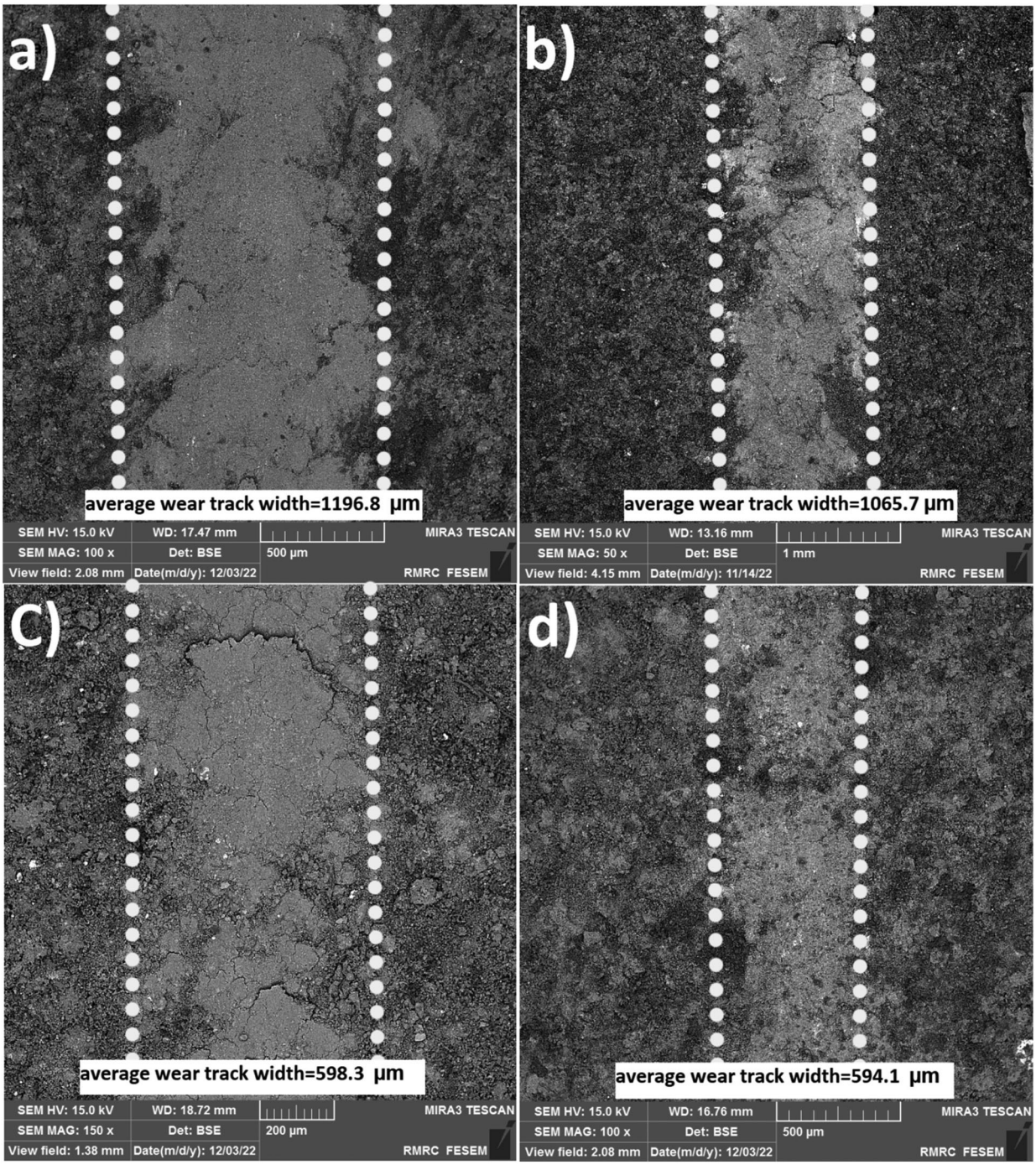

Figure 4. Hardness and wear rate of the coated specimens.

(TESCAN MIRA3, Czech Republic) equipped with an energy dispersive X-ray (EDX). EDS detector was employed to examine the delamination mechanism and the adhesive wear mechanism, which is affected by the transfer of tungsten element between coated surfaces and the WC pin during the wear test.

3. Results and discussion

3.1. Phase characterisation

The results of Rietveld refinement operated on the XRD patterns of the synthesised powders milled for 1.5, 3, and 6 h are presented in Figure 2(a–c) and Table 3. As seen, the reaction propagated completely and the final products of all the samples are Al_2O_3 and TiB_2. The combustion reaction duration was 60, 40, and 30 s for 1.5, 3, and 6 h milling time, respectively. It can be concluded that increasing milling time led to lower combustion reaction time in H_3BO_3, Al, and TiO_2 system. Moreover, the powders consist of about 70 wt% Al_2O_3 phase and about 30 wt.% TiB_2 phase, which is near to the calculated values of the products of the reaction (1), i.e.71 and 29 wt.% for Al_2O_3 and TiB_2, respectively. Therefore, for the next step, the 1.5 h milled composition was chosen to mix with SiC and then plasma spray on substrates.

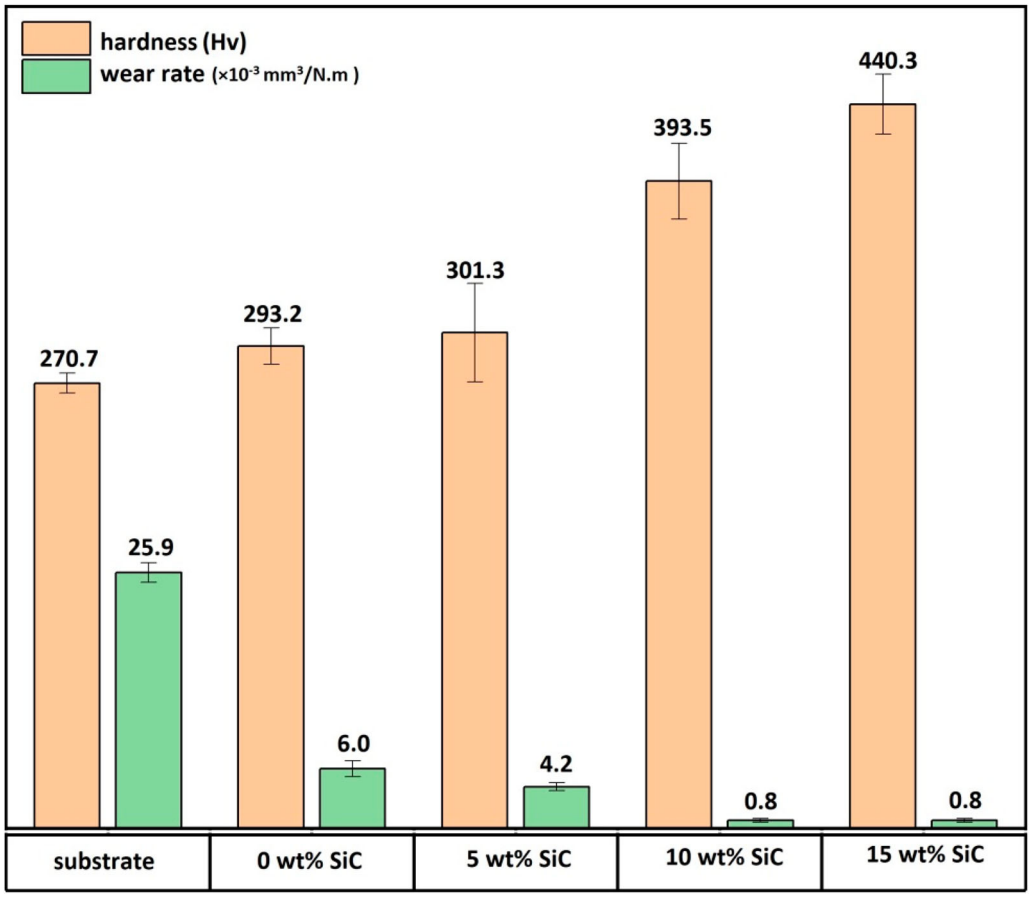

Figure 5. Wear track of the coated specimens: (a) C2, (b) C2-5S, (c) C2-10S, (d) C2-15S.

Figure 3 displays XRD patterns of the coated specimens, i.e. C2, C2-5S, C2-10S, and C2-15S. It was identified that after APS, α-Al_2O_3, and TiB_2 for C2 and α-Al_2O_3, TiB_2, and SiC for C2-5S, C2-10S and C2-15S were the detected phases. α-Al_2O_3 to the non-equilibrium γ-alumina transformation was observed for C2 and C2-5S. No phase transformation was observed for C2-10S and C2-15S after the plasma spray process, or the amount of in situ γ-alumina is not within the range that XRD can detect. Cheng et al. [19] reported α-alumina to γ-alumina phase transformation due to a high cooling rate during APS. Alvar et al. [21] have also reported α-alumina to γ-alumina phase transformation. There is also no TiO_2 phase peak in the XRD pattern which shows that TiB_2 oxidation probably did not occur. The theoretical thermal conductivity of SiC is larger than $300 W \cdot m^{1} \cdot K^{-1}$ at room temperature and is classified as a high thermal conductivity ceramic [35]. It can be said that the uniform distribution of SiC particles throughout the coated layer reduces the rapid cooling effect on the coating and prevents the creation of in situ and non-equilibrium phases. Moreover, SiC does not react with the other phases due to the non-reactivity of SiC, and the proportion of phases in composite remains approximately unchanged.

Table 4. Hardness of Al_2O_3-TiB_2 composites in comparison with other researches.

Material	Coating method	Hardness (Hv)	Reference
Al_2O_3-TiB_2-SiC	APS	440.3	Present work
Al_2O_3-TiB_2	IPS	520	[23,24]
Al_2O_3-TiB_2	APS	728–1668 620–1430	[19,20]
Al_2O_3-TiB_2	APS	1300	[10]
Al_2O_3-20wt%TiB_2	APS	1120	[21]
Al_2O_3-30wt%TiB_2	APS	1145	[21]
Al_2O_3-TiB_2-SiC_w	Bulk sample	2182–2243	[15]
Al_2O_3-TiB_2	Bulk nanocomposite	1642	[43]
TiB_2-SiC	APS	377.3	[27]
TiB_2-TiC-Al_2O_3-Al	IPS	254–723	[38]

3.2. Hardness and wear properties

The average surface roughnesses (R_a) of the coatings after plasma spray process were between 4 and 6 and 1 μm before wear test. Figure 4 depicts the FESEM image of the wear track of the coated specimens after the pin-on-disk test. In order to compare wear properties, two parameters of wear track width and wear rate must be specified. The average widths of the wear tracks and wear rates were calculated according to the attributed images. Based on the calculations, values of 1196.8, 1065.7, 598.3, and 594.1 μm were obtained for the width of the wear track of C2, C2-5S, C2-10S, and C2-15S, respectively. When the amount of SiC increased in the composition to 10 and 15 wt%, γ-alumina unwanted phase eliminated,

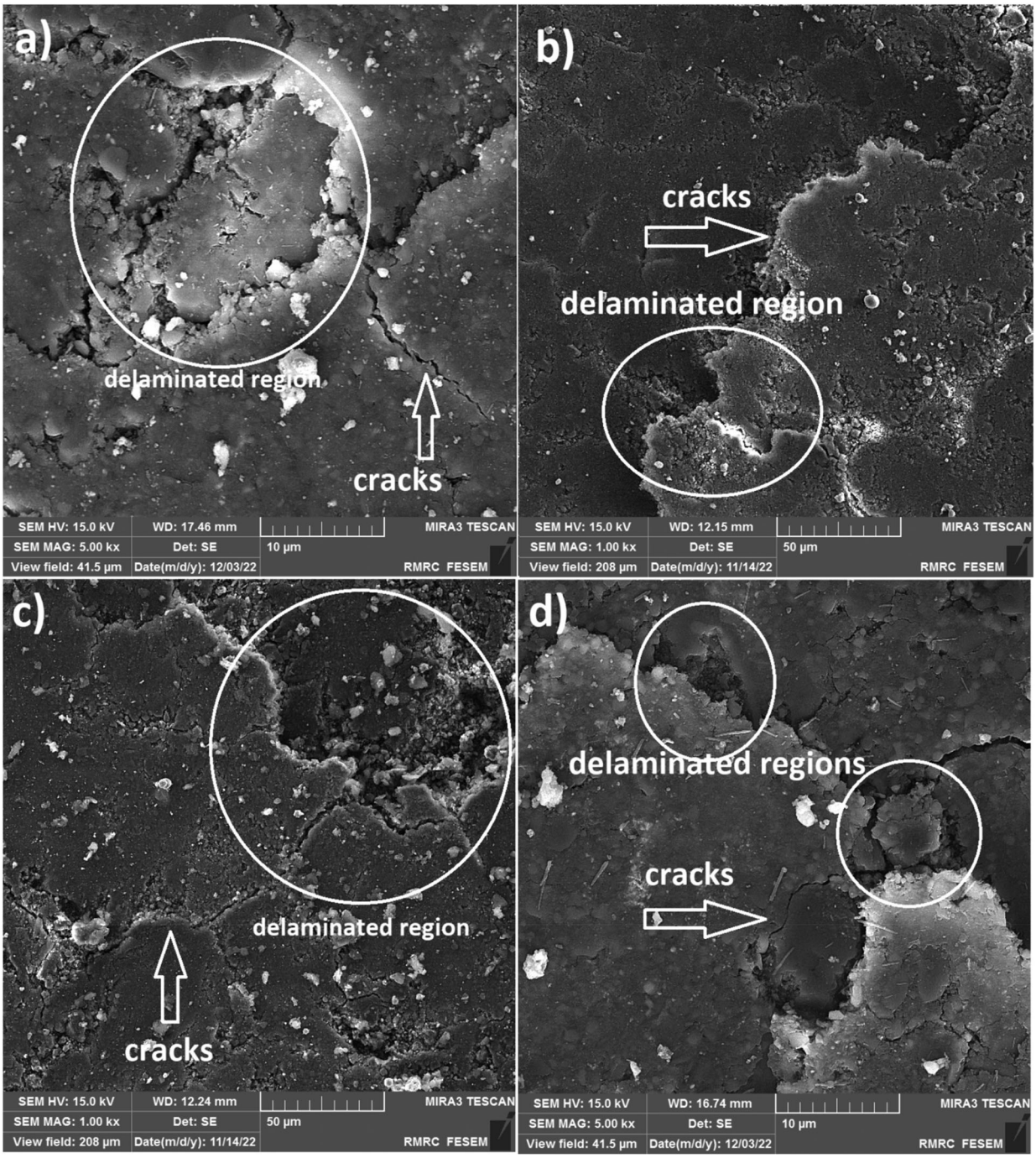

Figure 6. Higher magnification of worn surfaces of the coated specimens: (a) C2, (b) C2-5S, (c) C2-10S, (d) C2-15S.

and the wear track width reduced significantly. Wear rate is associated with Young's modulus, hardness, and fracture toughness of the composite. It was reported that adding SiC eliminated wear rate of bulk alumnia by blocking brittle fracture of the ceramic [36]. It seems that, in the Al_2O_3-TiB_2-SiC coating, SiC reduces crack propagation and growth. Notably, by the addition of 15 wt% SiC, the wear track width does not alter compared to the C2-10S sample. Seemingly, rising SiC content may lead to agglomeration and inhomogeneous microstructure. This can affect the wear properties and neutralise the positive effect of increasing SiC, which was the improvement of hardness and toughness of the coatings. Therefore, increasing SiC by 15 wt% does not make a significant change in the wear width.

Figure 5 illustrates composite coating hardness variation and wear rate versus SiC weight percentage. It is obvious that applying coating on the steel substrate led to a hardness improvement. As can be seen, adding SiC to the Al_2O_3-TiB_2 ceramic system led to increased hardness. The addition of SiC prevents the mobility of matrix grain boundaries defects [37]. The presence of SiC beside the Al_2O_3 grains and in the triple junctions suppresses the progress of defects by pining effect during plastic deformation [36]. Therefore, the addition of SiC increases the hardness of the coating.

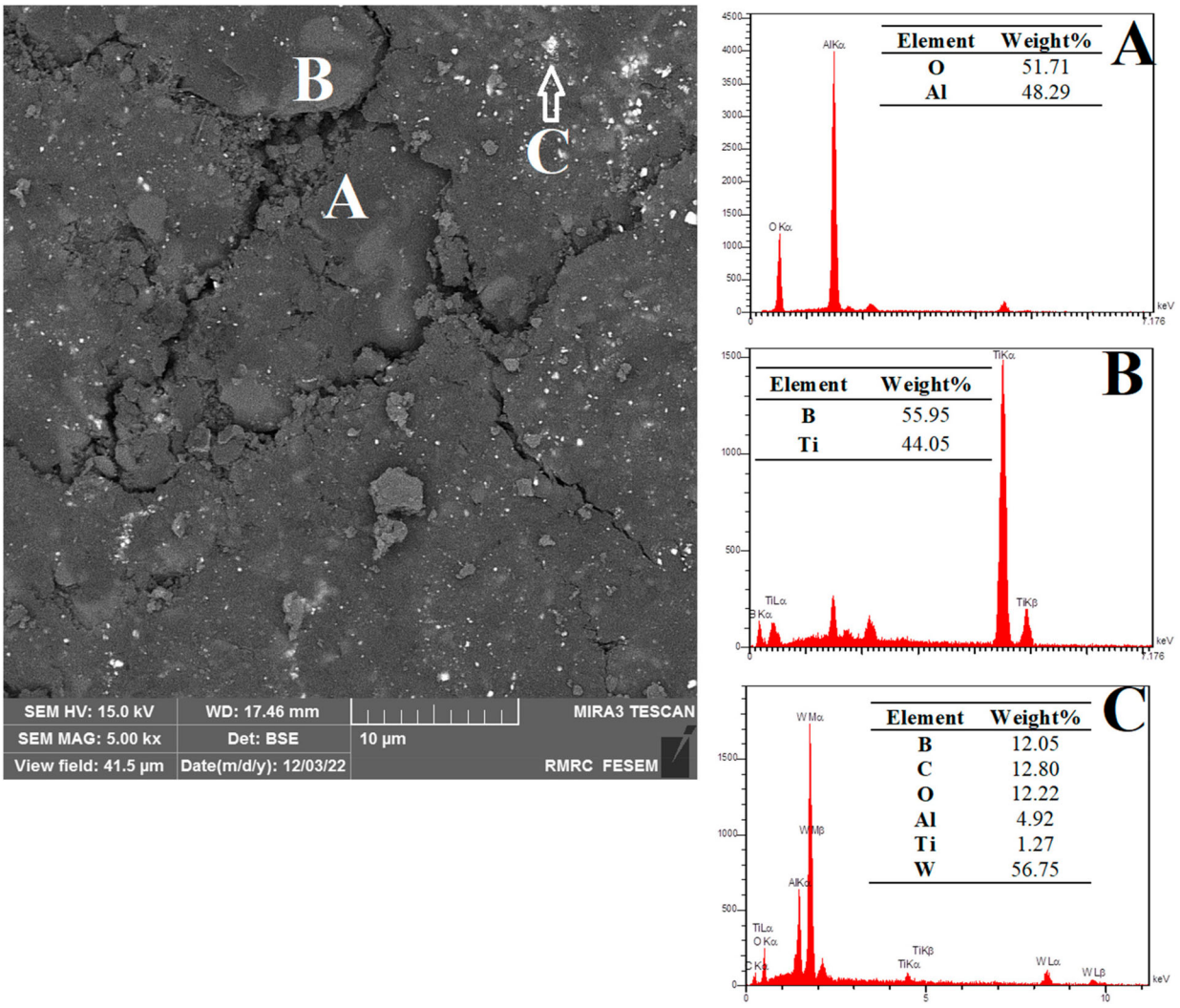

Figure 7. Microstructure and EDS analysis of C2 worn surface.

Tekmen et al. [23,24] produced in-situ plasma sprayed Al_2O_3-TiB_2 coating with 520 $Hv_{0.2}$. Cheng et al. [19,20] reported hardness values of APSed coatings fabricated by Al_2O_3-TiB_2 SHSed powders in the range of 728–1668 Hv and 620–1430 Hv with 100 and 200 g load For plasma sprayed Al_2O_3-TiB_2. In another study, reactive plasma sprayed Al_2O_3-TiB_2 with a hardness of 1300 $Hv_{0.1}$ was developed [10]. Alvar et al. [21] studied Al_2O_3-TiB_2 nanocomposite coatings and declared 1120 and 1145 for 20 and 30 wt% of TiB_2, respectively. Jianxin [15] investigated the hardness of hot-pressed Al_2O_3-TiB_2-SiC_w bulk and reported 2182–2243 Hv hardness. In another study, IPSed (in-situ plasma sprayed) TiB_2-TiC-Al_2O_3-Al coating was obtained 254-723Hv [38]. These results are summarised in Table 4. Notably, the hardness of Al_2O_3-TiB_2 coating is lower than its nanocomposite coating and bulk. Finer particles, especially in nanocomposites resist more against plastic deformation due to more grain boundaries, so the hardness is more than bodies with coarse particles [37]. The lower value of the hardness of the Al_2O_3-TiB_2 may be due to remaining unmolten materials, microcracks, and higher porosity [2,39].

It is clear that SiC reinforcement has an essential role in the reduction of the wear rate of coated samples. It can be noticed that the wear rates of C2-10S and C2-15S are the same, because the wear track widths of them are similar. For a hot-pressed Al_2O_3-TiB_2-SiC_w bulk specimen, the wear rate is calculated as less than 10^{-7} mm^3/N.m with Vickers hardness of about 2213 and 2243 for 20 and 30 wt% SiC whiskers [15]. In another research, $H_V = 2714$ and a wear rate of $0.126 \times 10^{-3}(mm^3/N.m)$ for an Al_2O_3-TiB_2-TiN composite coating produced by Laser surface alloying [8]. Dey et al. [40] have also reported a wear rate of $0.557 \times 10^{-3}(mm^3/N.m)$ for Al_2O_3-TiB_2-TiN-BN composite coating ($H_V = 492.35$) and $0.376 \times 10^{-3}(mm^3/N.m)$ with $H_V = 1052.19$ for another sample which were developed by laser cladding method. These results show that the wear rate depends on the hardness of the surface severely. The porosity of the composite has a direct impact on its Elastic module (E). Present results show less hardness compared

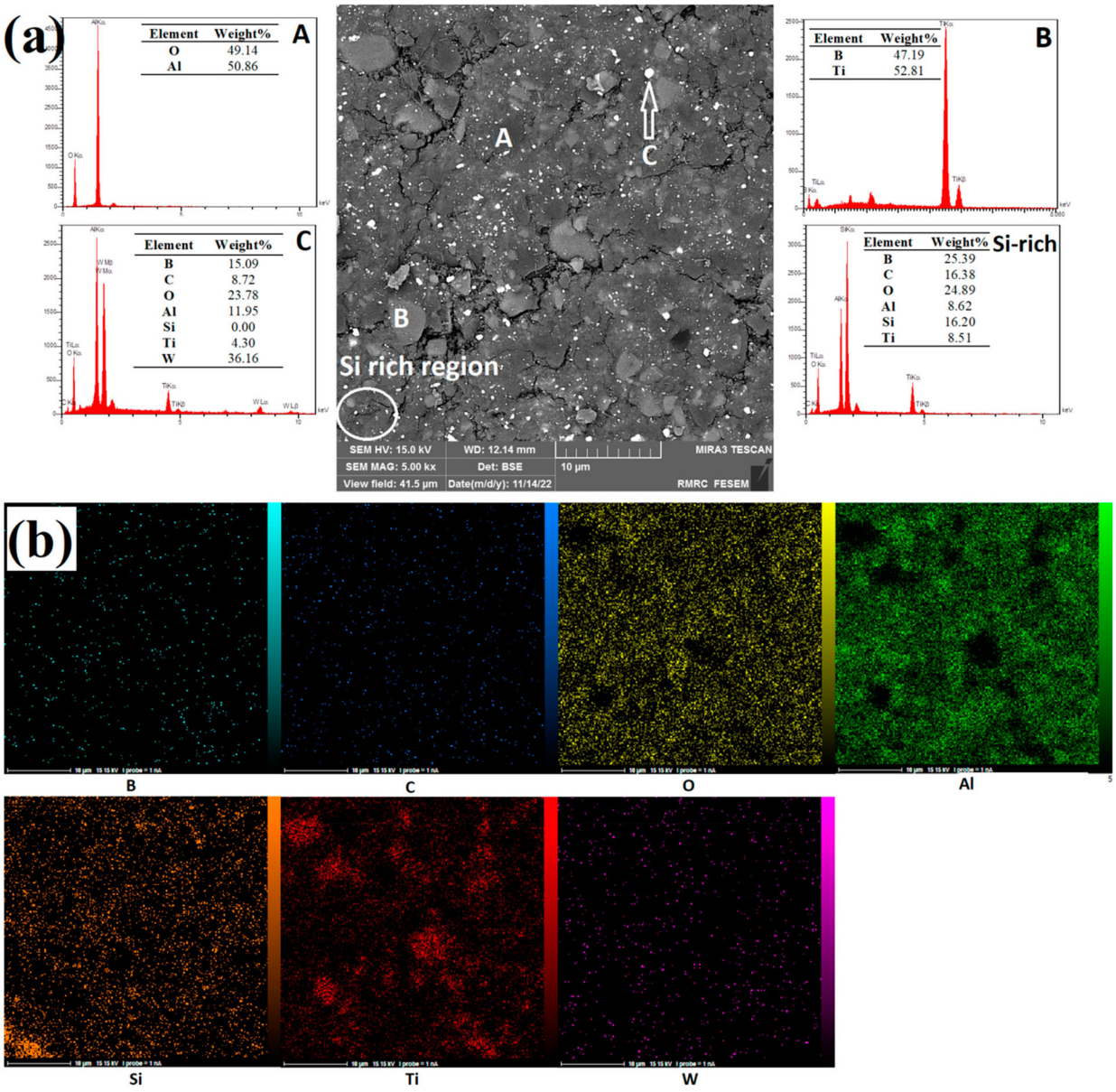

Figure 8. (a) Microstructure and EDS analysis, (b) Map analysis of C2-5S worn surface.

to previous works and more porosity, consequently. When porosity exceeds, E will decrease and will increase the H/E ratio, which improves wear resistance [41,42]. In summary, although the hardness of Al_2O_3-TiB_2-SiC of the present work is lower than the hardness of Al_2O_3-TiB_2, H/E growth improves wear resistance.

3.3. Microstructure evaluations of worn surfaces

Figure 6 shows higher magnification secondary electron images of worn surfaces of the coated specimens. As seen, several microcracks grew on the surface of the coated samples (Figure 6(a–d)). Ceramic composites are brittle and have low fracture toughness, and cracks can create and grow during pin-on-disk experiment. It can be said that the brittle fracture mechanism has an important role in all of the samples and may be originated from fatigue [44]. These microcracks meet each other and lead to the creation of delaminated regions (Figure 6(a–d)). Finally, the delamination mechanism occurs during the wear experiment [45]. Coefficient of thermal expansion (CTE) of Al_2O_3, TiB_2 and SiC are 9.08×10^{-6}, 8.1×10^{-6}, and 5.48×10^{-6} $°C^{-1}$, respectively [16]. The entry of SiC particles into the Al_2O_3-TiB_2 coating causes residual compressive stress due to a mismatch of the coefficient of thermal expansion on the SiC/Al_2O_3 and SiC/TiB_2 grain interfaces, and the interface bonding strength improves. On the other hand, the tensile stress of the Al_2O_3 matrix increases. Therefore, the fracture toughness enhances, because the crack needs more energy to propagate along the interfaces. Additionally, the presence of SiC particles can reduce crack energy by increasing the crack path length. SiC particles can also pin cracks, and prohibit crack development [46]. At last, the fracture toughness increases

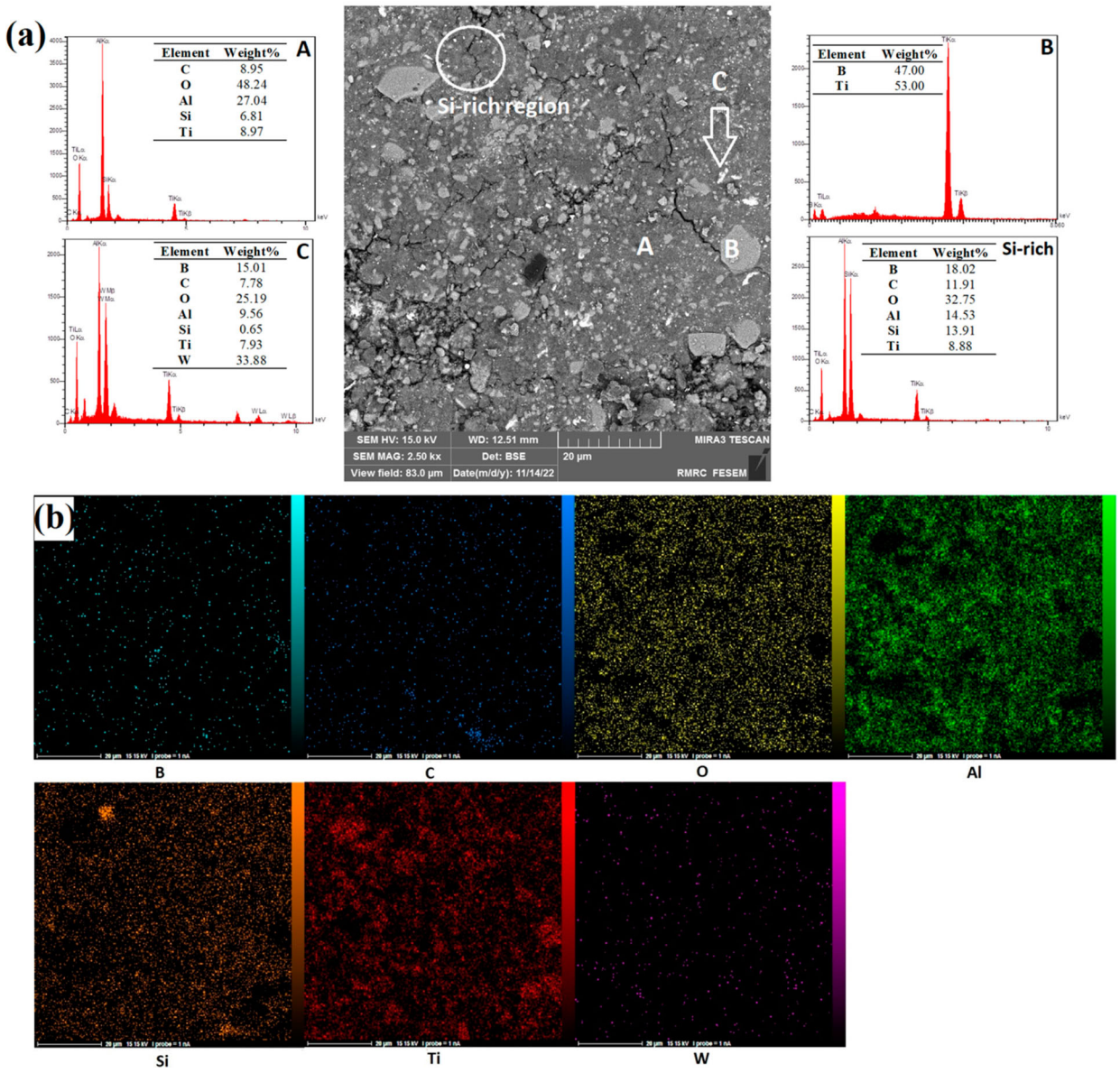

Figure 9. (a) Microstructure and EDS and (b) MAP analysis of C2-10S worn surface.

and the wear behaviour of the ternary composite coatings enhances.

Figures 7 and 8 show the microstructure of worn surfaces of C2 and C-5S coatings. EDS analysis was applied to investigate elemental evaluation. The grey matrix (point A) is Al_2O_3 and the light grey phase (point B) is TiB_2. It was difficult to distinguish the SiC phase due to the similar colour contrast with Al_2O_3. With the aid of map analysis (Figure 8(b)), a Si-rich region was found. White particles (point C) are rich in tungsten element originating from the WC pin test. It confirms that during the wear test, movement of the hard pin on the coating surface led to WC particles removal and adhesive wear mechanism occurred. The hardness of SiC is more than WC and TiB_2 is harder than WC due to its ionic-covalent bonding [47]. During the wear test of the Al_2O_3-TiB_2 coatings, the WC pin contacts TiB_2 and SiC phase, and WC particles separate. Moreover, removed WC particles on the wear track can perform as an abrasive agent and make more particles from WC pin separated. Therefore, the detached WC particles stick to the wear surface [45]. As it can be seen, more WC particles are on the C2-5S worn surface compared to C2. This can be related to the higher hardness of C2-5S due to higher SiC content.

Figure 9 shows the microstructure and map analysis of the C2-10S worn surface. Point A shows the alumina matrix, and point B is TiB_2. Scattered WC white particles (point C) adhere to the worn surface. As can be seen, wherever the O element exists, Si also exists. Moreover, the C element does not exist to a large extent. Consequently, it can be said that during the wear test in the air atmosphere, due to the movement of the pin on the coating, the surface of the SiC grains is scratched. On the other hand, wear tensions create some cracks on the surface. Therefore, oxygen can penetrate through the

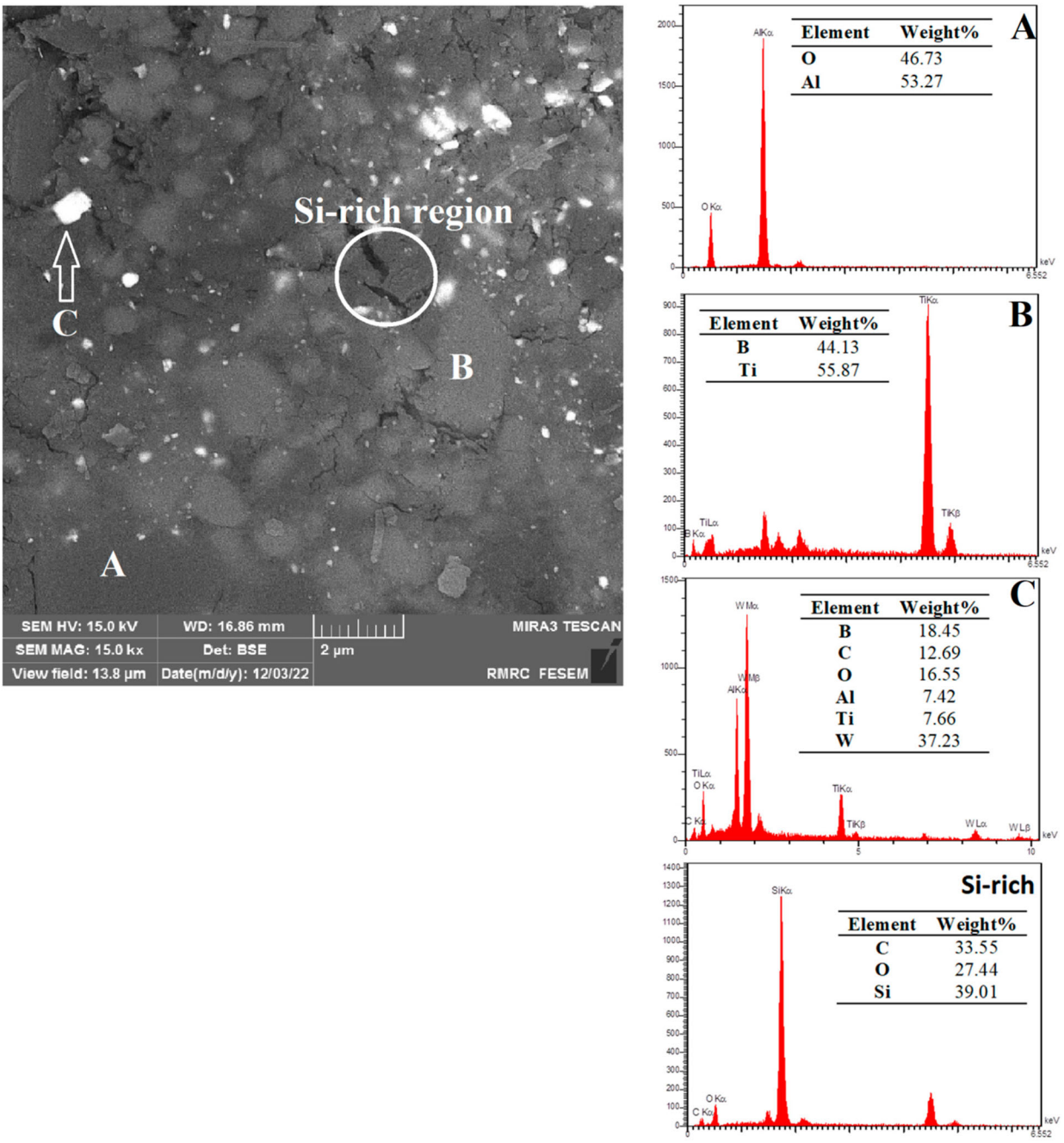

Figure 10. (a) Microstructure and EDS analysis of (b) Map analysis C2-15S worn surface.

imperfect surface and cracks, SiC partially oxidises and transforms to SiO_2 in some extent.

The microstructure of the C2-15S worn surface is shown in Figure 10. As stated before, according to EDS results, points A and B refer to alumina and TiB_2, respectively. WC separated particles (point C) scattered through the worn surface. As SiC content increase, more SiC hard particles will face to WC pin and more WC will remove. According to worn surface figures, white WC particles are exceeded from C2 to C2-15S. As seen, in the Si-rich region, SiC grains partially oxidised, and the EDS analysis showed Si, C, and O elements. A crack has also grown in the middle of the Si-rich region which can provide a path for oxygen entrance. In conclusion, the oxidation mechanism can be activated during the pin on disk wear test of SiC-containing coatings. Gupta and Kumar [48] reported the reaction of SiC with air oxygen during the wear test for ZrB_2-SiC composite based on reaction (2). Related tribooxidation occurrence has also been declared by other studies [49,50].

$$SiC + 1.5O_2 = SiO_2 + CO \quad (2)$$

Figure 11(a) depicts the C2-10S cross section and Figure 11(b) shows a higher magnification of the coating layer. The coating, interface layer, and substrate are observed in Figure 11(a). As seen, the NiCrAlY layer is well deposited onto the substrate. Additionally,

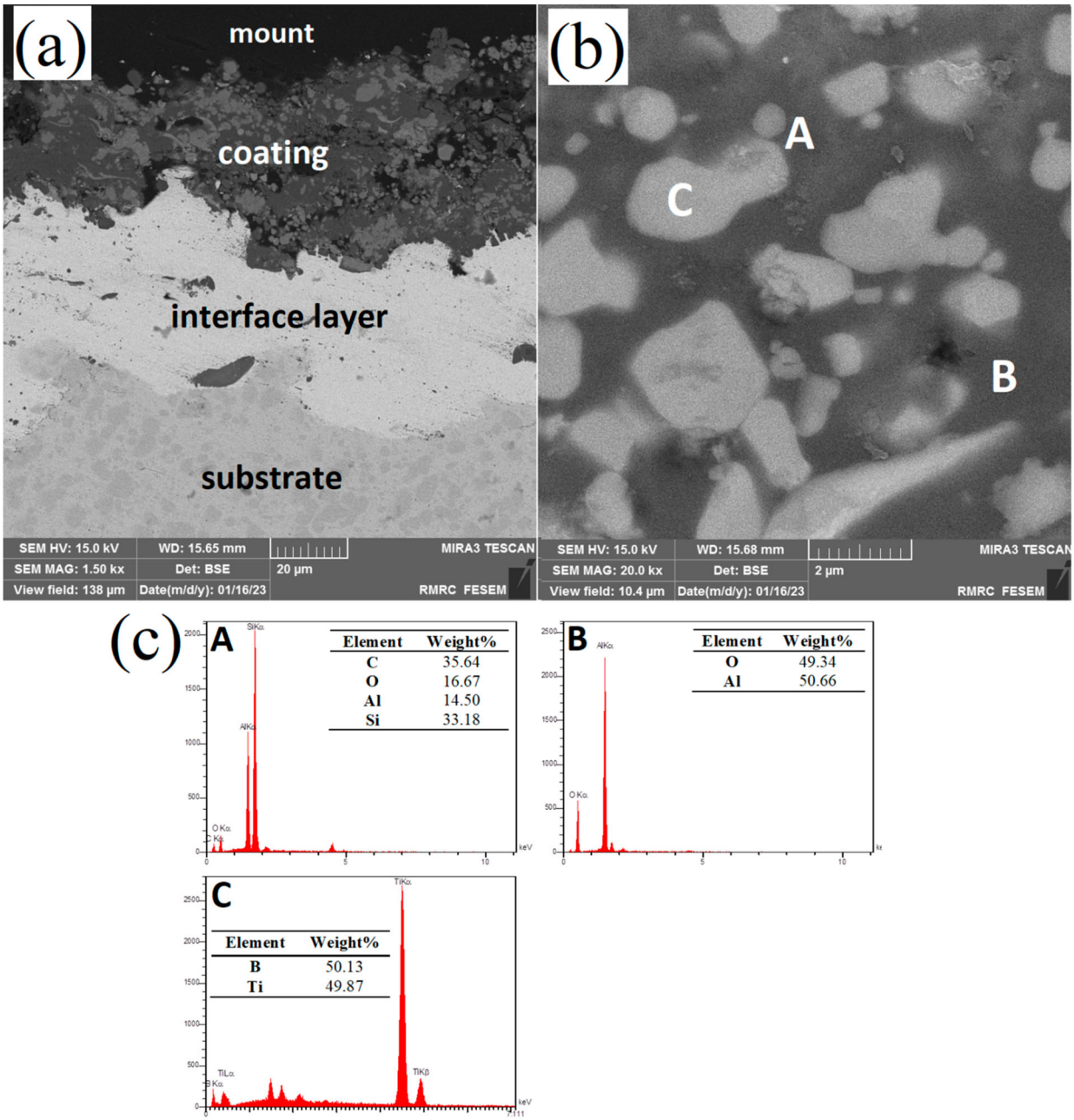

Figure 11. (a) Cross section of C2-10S, (b) C2-10S surface coating layer at higher magnification, (c) EDS analysis of different phases.

Good adherence between the composite coating and the interface layer is achieved. According to EDS analysis of different phases (Figure 11(c)), point A is related to the SiC phase, B to Al_2O_3, and C to TiB_2, and distribution of reinforcements throughout the composite layer is uniform.

3.4. Friction behaviour

Figure 12 reveals the variation of the friction coefficient (COF) with the sliding distance obtained from pin-on-disk experiments for the coated specimens. Normally, COF graphs can be identified by two parameters, i.e. μ_p and μ_{ss}, which are COF at peak value and COF at steady state value, respectively. COF values are 1.73, 2.91, 2.88, 2.16, and 0.81 for substrate, C2, C2-5S, C2-10S, and C2-15S, respectively. As seen, the 10 wt% SiC and 15 wt% SiC composite coatings showed more stable friction and wear behaviour than that of the Al_2O_3-TiB_2 and 5 wt% SiC ceramic coatings. SiC particles played a role as a solid lubricant in this tribological composite system, enhancing the friction and wear characteristics of the coatings [51]. It is clear that adding 10 wt% SiC and 15 wt% SiC can reduce the fluctuation of COF curves and help the wear resistance. Zhou et al. have reported Ni-SiC coating showed a more stable curve of COF in comparison with Ni coating [52]. Moreover, adding 15 wt. % SiC did not change wear rate, but it decreased COF significantly. It is assumed that the self-lubricanting feature of SiC activates by 15%wt. COF reduction can be attributed to SiO_2 phase formation, which is

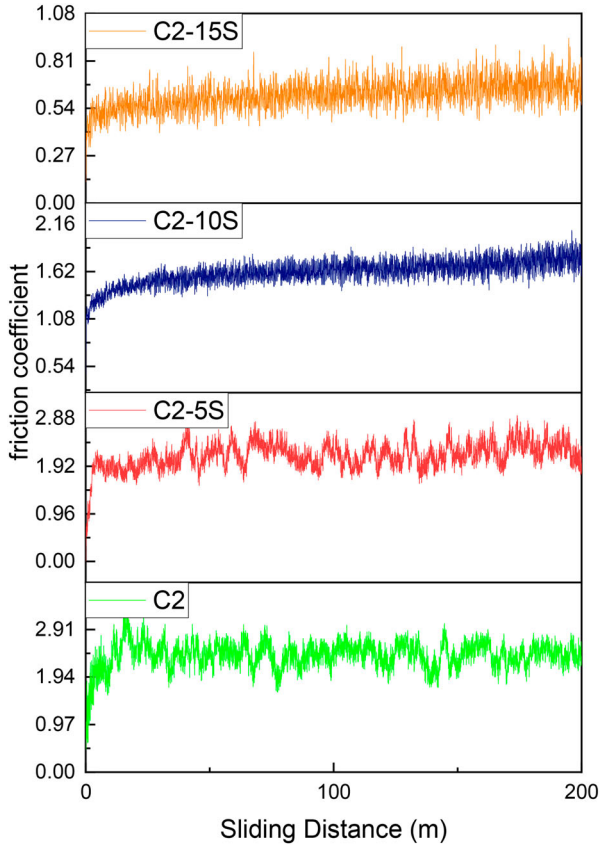

Figure 12. Variation of friction coefficient with the sliding distance for the coated specimens.

more notable in C2-15S. Zhang et al. [53] also investigated SiC lubrication by annealing in atmospheric condition and demonstrated that the creation of SiO_2 layers minimise COF and improve the wear resistance of SiC. Deng et al. [44] also stated that due to the reaction of silica with air humidity, colloidal silica is formed based on reaction (3), which is an effective lubricant product. By increasing the amount of SiC to 15%%wt., more SiO_2 phase and colloidal silica are produced, and the friction coefficient drops significantly. In conclusion, oxidation and silica phase reveal the anti-fluctuation effect of SiC in C2-10S and C2-15S samples.

$$SiO_2 + 2H_2O = Si(OH)_4 \quad (3)$$

4. Conclusions

In this study, the air plasma spray method was utilised to create Al_2O_3-TiB_2-SiC composite coatings on steel substrates using the SHS-synthesised powders. The effects of SiC reinforcement content on the microstructure and wear behaviour of the coatings were then evaluated. The key findings from the experiments and analysis can be summarised as follows:

1. SiC reinforcing agent was used for Al_2O_3-TiB_2 composite coatings on steel substrates to improve wear properties successfully. Phase transformation from α-alumina to γ-alumina did not occur after the plasma spray process.
2. SiC reinforcement improves wear resistance by increasing hardness, mitigating cracks energy, less wear track width, and less wear rate.
3. Based on the wear rate results, the Al_2O_3-TiB_2-10% SiC composite has the lowest wear volume rate. Interestingly, 10 SiC and 15 wt% can activate the anti-fluctuation effect of SiC, according to COF graphs. Adding 15 wt% SiC did not change the wear rate, but it decreased COF significantly through SiO_2 lubricant phase formation.
4. Principal wear mechanisms are brittle fracture, adhesive, and delamination. Through EDS analysis, it can be drawn that the SiC tribo-oxidation mechanism during the wear test plays a vital role in COF reduction and wear resistance.

Disclosure statement

No potential conflict of interest was reported by the author(s).

References

[1] Gupta A, Pattnayak A, Abhijith NV, et al. Development of alumina-based hybrid composite coatings for high temperature erosive and corrosive environments. Ceram Int. 2023;49(1):862–874. doi:10.1016/j.ceramint.2022.09.059

[2] Sarikaya O. Effect of some parameters on microstructure and hardness of alumina coatings prepared by the air plasma spraying process. Surf Coat Technol. 2005;190(2–3):388–393. doi:10.1016/j.surfcoat.2004.02.007

[3] Grewal HS, Singh H, Agrawal A. Microstructural and mechanical characterization of thermal sprayed nickel–alumina composite coatings. Surf Coat Technol. 2013;216:78–92. doi:10.1016/j.surfcoat.2012.11.029

[4] Masanta M, Shariff SM, Choudhury AR. Tribological behavior of TiB_2–TiC–Al_2O_3 composite coating synthesized by combined SHS and laser technology. Surf Coat Technol. 2010;204(16–17):2527–2538. doi:10.1016/j.surfcoat.2010.01.027

[5] Masanta M, Shariff SM, Choudhury AR. Evaluation of modulus of elasticity, nano-hardness and fracture toughness of TiB_2–TiC–Al_2O_3 composite coating developed by SHS and laser cladding. Mater Sci Eng A. 2011;528(16–17):5327–5335. doi:10.1016/j.msea.2011.03.057

[6] Chatterjee S, Shariff SM, Padmanabham G, et al. Study on the effect of laser post-treatment on the properties of nanostructured Al_2O_3–TiB_2–TiN based coatings developed by combined SHS and laser surface alloying. Surf Coat Technol. 2010;205(1):131–138. doi:10.1016/j.surfcoat.2010.06.015

[7] Li Z, Wei M, Xiao K, et al. Microhardness and wear resistance of Al_2O_3-TiB_2-TiC ceramic coatings on carbon steel fabricated by laser cladding. Ceram Int. 2019;45(1):115–121. doi:10.1016/j.ceramint.2018.09.140

[8] Chatterjee S, Majumdar JD, Singaiah K, et al. Performance evaluation of laser surface alloyed hard

nanostructured Al2O3–TiB2–TiN composite coatings with in-situ and ex-situ reinforcements. Surf Coat Technol. 2011;205(11):3478–3484. doi:10.1016/j.surfcoat.2010.12.015

[9] Ko YM, Kwon WT, Kim Y-W. Development of Al_2O_3–SiC composite tool for machining application. Ceram Int. 2004;30(8):2081–2086. doi:10.1016/j.ceramint.2003.11.011

[10] Zhou XP, Li M, Zhou X. Process study on prepared Al_2O_3-TiB_2 composite coating by reactive spray. Adv Mater Res. 2012;472:309–312. doi:10.4028/www.scientific.net/AMR.472-475.309

[11] Smirnov BI, Nikolaev VI, Burenkov YA, et al. Some physical properties of an Al_2O_3-SiC-TiC composite. Tech Phys Lett 1997;23(12):923–926. doi:10.1134/1.1261934

[12] Smirnov BI, Nikolaev VI, Orlova TS, et al. Mechanical properties and microstructure of an Al_2O_3–SiC–TiC composite. Mater Sci Eng A. 1998;242(1–2):292–295. doi:10.1016/S0921-5093(97)00744-2

[13] Nallusamy T. High-temperature stability of titanium boride reinforced alumina-silicon carbide based composite. Silicon. 2021;13(4):1087–1095. doi:10.1007/s12633-020-00498-y

[14] Jianxin D, Xing A. Sic whisker reinforced Al_2O_3/TiB_2 ceramic composites. Chin Ceram Soc. 1995;23(4):385–392.

[15] Jianxin D. Friction and wear behaviour of Al_2O_3/TiB_2/SiCw ceramic composites at temperatures up to 800 C. Ceram Int 2001;27(2):135–141. doi:10.1016/S0272-8842(00)00052-3

[16] Masanta M, Ganesh P, Kaul R, et al. Microstructure and mechanical properties of TiB_2–TiC–Al_2O_3–SiC composite coatings developed by combined SHS, sol–gel and laser technology. Surf Coat Technol. 2010;204(21–22):3471–3480. doi:10.1016/j.surfcoat.2010.04.018

[17] Ali A, Ahmad SN. Mechanical and tribological behavior of TiB_2/Al_2O_3 coating on high-speed steel using electron beam deposition. Tribol Int 2022;174:107681. doi:10.1016/j.triboint.2022.107681

[18] Masanta M, Shariff SM, Choudhury AR. A comparative study of the tribological performances of laser clad TiB_2–TiC–Al_2O_3 composite coatings on AISI 1020 and AISI 304 substrates. Wear. 2011;271(7–8):1124–1133. doi:10.1016/j.wear.2011.05.009

[19] Cheng HC, Li ZX, Shi YW. Microstructure and wear resistance of Al_2O_3–TiB_2 composite coating deposited by axial plasma spraying. Surf Eng 2008;24(6):452–457. doi:10.1179/026708408X334122

[20] Cheng HC, Li ZX, Shi YW. Effects of TIG surface treating on microstructural characteristics and mechanical properties of Al_2O_3–TiB_2 coating by APS. Mater Sci Technol. 2011;27(1):194–200. doi:10.1179/174328409X418946

[21] Alvar FS, Heydari M, Kazemzadeh A, et al. Synthesis and characterization of corrosion-resistant and biocompatible Al_2O_3–TiB_2 nanocomposite films on pure titanium. Ceram Int. 2020;46(4):4215–4221. doi:10.1016/j.ceramint.2019.10.140

[22] Alvar FS, Heydari M, Kazemzadeh A, et al. Al_2O_3-TiB_2 nanocomposite coating deposition on titanium by air plasma spraying. Mater Today Proc. 2018;5(7):15739–15743. doi:10.1016/j.matpr.2018.04.186

[23] Tekmen C, Tsunekawa Y, Okumiya M. In-situ TiB_2 and Al_2O_3 formation by DC plasma spraying. Surf Coat Technol. 2008;202(17):4170–4175. doi:10.1016/j.surfcoat.2008.03.012

[24] Tekmen C, Tsunekawa Y, Okumiya M. In-situ TiB_2–Al_2O_3 formed composite coatings by atmospheric plasma spraying: influence of process parameters and in-flight particle characteristics. Surf Coat Technol. 2009;203(12):1649–1655. doi:10.1016/j.surfcoat.2008.12.016

[25] Di Girolamo G, Brentari A, Blasi C, et al. Microstructure and mechanical properties of plasma sprayed alumina-based coatings. Ceram Int. 2014;40(8):12861–12867. doi:10.1016/j.ceramint.2014.04.143

[26] Xu J, Zou B, Tao S, et al. Fabrication and properties of Al_2O_3–TiB_2–TiC/Al metal matrix composite coatings by atmospheric plasma spraying of SHS powders. J Alloys Compd 2016;672:251–259. doi:10.1016/j.jallcom.2016.02.116

[27] Zou K, Zou JP, Deng CM, et al. Preparation and properties of supersonic atmospheric plasma sprayed TiB_2–SiC coating. Trans Nonferrous Met Soc China. 2021;31(1):243–254. doi:10.1016/S1003-6326(20)65491-7

[28] Luo P, Dong S, Yangli A, et al. Electrospark deposition of Al_2O_3–TiB_2/Ni composite-phase surface coatings on Cu–Cr–Zr alloy electrodes. J Asian Ceram Soc. 2015;3(1):103–107. doi:10.1016/j.jascer.2014.11.005

[29] Mousavian RT, Sharafi S, Roshan MR, et al. Effect of mechanical activation of reagents' mixture on the high-temperature synthesis of Al_2O_3–TiB_2 composite powder. J Therm Anal Calorim 2011;104(3):1063–1070. doi:10.1007/s10973-010-1272-0

[30] Yeh CL, Li RF. Formation of TiB_2–Al_2O_3 and NbB_2–Al_2O_3 composites by combustion synthesis involving thermite reactions. Chem Eng J 2009;147(2–3):405–411. doi:10.1016/j.cej.2009.01.007

[31] Meyers MA, Olevsky EA, Ma J, et al. Combustion synthesis/densification of an Al_2O_3–TiB_2 composite. Mater Sci Eng A. 2001;311(1–2):83–99. doi:10.1016/S0921-5093(01)00930-3

[32] Standard A. G99, Standard test method for wear testing with a pin-on-disk apparatus. West Conshohocken (PA): ASTM Int.; 2006.

[33] Li X, Olofsson U, Bergseth E. Pin-on-disc study of tribological performance of standard and sintered gear materials treated with triboconditioning process: pretreatment by pressure-induced tribofilm formation. Tribol Trans 2017;60(1):47–57. doi:10.1080/10402004.2016.1146379

[34] Ardiani NR, Setianto S, Santosa B, et al. Quantitative analysis of iron sand mineral content from the south coast of cidaun, west java using rietveld refinement method. AIP Conf Proc. 2020;2219(1):40003. doi:10.1063/5.0003018

[35] Watari K. High thermal conductivity non-oxide ceramics. J Ceram Soc Japan. 2001;109(1265):S7–S16. doi:10.2109/jcersj.109.S7

[36] Limpichaipanit A, Todd RI. The relationship between microstructure, fracture and abrasive wear in Al_2O_3/SiC nanocomposites and microcomposites containing 5 and 10% SiC. J Eur Ceram Soc. 2009;29(13):2841–2848. doi:10.1016/j.jeurceramsoc.2009.03.023

[37] Krell A. A new look at the influences of load, grain size and grain boundaries on the room temperature hardness of ceramics. Int J Refract Met Hard Mater. 1998;16(4–6):331–335. doi:10.1016/S0263-4368(98)00056-0

[38] Xu J, Zou B, Fan X, et al. Reactive plasma spraying synthesis and characterization of TiB_2–TiC–Al_2O_3/Al composite coatings on a magnesium alloy. J Alloys Compd. 2014;596:10–18. doi:10.1016/j.jallcom.2014.01.178

[39] Pantelis DI, Psyllaki P, Alexopoulos N. Tribological behaviour of plasma-sprayed Al_2O_3 coatings under severe wear conditions. Wear. 2000;237(2):197–204. doi:10.1016/S0043-1648(99)00324-5

[40] Dey D, Bal KS, Khan I, et al. Study of tribo-mechanical properties of laser clad Al_2O_3-TiB_2-TiN-BN‖ Ti-6Al-4 V alloy. Opt Laser Technol. 2022;150:107982. doi:10.1016/j.optlastec.2022.107982

[41] Gudlur P, Forness A, Lentz J, et al. Thermal and mechanical properties of Al/Al_2O_3 composites at elevated temperatures. Mater Sci Eng A. 2012;531:18–27. doi:10.1016/j.msea.2011.10.001

[42] Leyland A, Matthews A. On the significance of the H/E ratio in wear control: a nanocomposite coating approach to optimised tribological behaviour. Wear. 2000;246(1–2):1–11. doi:10.1016/S0043-1648(00)00488-9

[43] Rabiezadeh A, Ataie A, Hadian AM. Sintering of Al_2O_3–TiB_2 nano-composite derived from milling assisted sol–gel method. Int J Refract Met Hard Mater. 2012;33:58–64. doi:10.1016/j.ijrmhm.2012.02.013

[44] Deng W, Li S, Hou G, et al. Comparative study on wear behavior of plasma sprayed Al_2O_3 coatings sliding against different counterparts. Ceram Int. 2017;43(9):6976–6986. doi:10.1016/j.ceramint.2017.02.122

[45] Khorsand A, Majidian H, Farvizi M. Wear behavior and microstructure of alumina-mullite-zirconia composites prepared by a novel method: coating of zircon powder by aluminum alkoxide. Ceram Int. 2022;48(22):33594–33603. doi:10.1016/j.ceramint.2022.07.304

[46] Wu D, Lu F, Zhao D, et al. Effect of doping SiC particles on cracks and pores of Al_2O_3–ZrO_2 eutectic ceramics fabricated by directed laser deposition. J Mater Sci. 2019;54(13):9321–9330. doi:10.1007/s10853-019-03555-z

[47] Basu B, Kalin M. Tribology of ceramics and composites: a materials science perspective. United Kingdom: John Wiley & Sons; 2011.

[48] Gupta Y, Kumar BVM. Zrb_2–SiC composites for sliding wear contacts: influence of SiC content and counterbody. Ceram Int. 2022;48(10):14560–14567. doi:10.1016/j.ceramint.2022.01.349

[49] Sengupta P, Basu S, Manna I. Comparative evaluation of TiC and/or WC addition on microstructure, mechanical properties, thermal residual stress and reciprocating wear behaviour of ZrB_2–20SiC composites. J Mater Sci. 2023;58:420–442. doi:10.1007/s10853-022-08021-x

[50] Savchenko N, Mirovoy Y, Burlachenko A, et al. Subsurface multilayer evolution of ZrB_2–SiC ceramics in high-speed sliding and adhesion transfer conditions. Wear. 2021;482:203956. doi:10.1016/j.wear.2021.203956

[51] Dong Y, Yan D, He J, et al. Dry sliding wear behavior of ceramic-metal composite coatings prepared by plasma spraying of self-reacting powders. J Therm Spray Technol. 2006;15:323–328. doi:10.1361/105996306X92541

[52] Zhou Y, Zhang H, Qian B. Friction and wear properties of the co-deposited Ni–SiC nanocomposite coating. Appl Surf Sci. 2007;253(20):8335–8339. doi:10.1016/j.apsusc.2007.04.047

[53] Zhang W, Yamashita S, Kita H. Self lubrication of pressureless sintered SiC ceramics. J Mater Res Technol. 2020;9(6):12880–12888. doi:10.1016/j.jmrt.2020.09.022